

# Diagnostic Signatures of Radio and HXR Emission on Particle Acceleration Processes in the Coma Cluster

Ping-Hung Kuo, Chorng-Yuan Hwang, and Wing-Huen Ip

*Institute of Astronomy, National Central University, Chung-Li 32054, Taiwan*

d882001@astro.ncu.edu.tw, hwangcy@astro.ncu.edu.tw, wingip@astro.ncu.edu.tw

## ABSTRACT

We investigate theoretical models for the radio halo and hard X-ray (HXR) excess in the Coma galaxy cluster. Time-independent and time-dependent re-acceleration models for relativistic electrons have been carried out to study the formation of the radio halo and HXR excess. In these models, the relativistic electrons are injected by merger shocks and re-accelerated by ensuing violent turbulence. The effects of different Mach numbers of the merger shocks on the radio and HXR excess emission are also investigated. We adopt  $6 \mu\text{G}$  as the central magnetic field and reproduce the observed radio spectra via the synchrotron emission. We also obtain a central “plateau” in the radio spectral-index distribution, which have been observed in radio emission distribution. Our models can also produce the observed HXR excess emission via the inverse Compton scattering of the cosmic microwave background photons. We find that only the merger shocks with the Mach numbers around 1.6–2 can produce results in agreement with both the radio and HXR emission in the Coma cluster.

*Subject headings:* galaxies: clusters: individual (Coma) — magnetic fields — radiation mechanisms: non-thermal — radio continuum: general — X-rays: general

## 1. INTRODUCTION

Radio halos in galaxy clusters are diffuse radio sources possessing large sizes and steep spectra. The radio emission must be produced by the synchrotron radiation of relativistic electrons. Nonetheless, the sources of these relativistic electrons are still unclear. In the intracluster medium (ICM), relativistic electrons lose energy on the time scale of order  $\sim 10^8$  years because of inverse Compton and synchrotron losses (e.g., Ip & Axford 1999). Because

of the short lifetimes of the relativistic electrons, it is difficult to interpret the large size of radio halos as the result of the diffusion of the relativistic electrons injected from radio galaxies (Jaffe 1977). Consequently, for the formation of radio halos, a significant level of re-acceleration might be involved. The secondary electron model first proposed by Dennison (1980) provides a different scenario for the origin of the radio halo and can avoid the problem of re-acceleration for the relativistic electrons in the primary electron models. However, this model encounters serious problems when comparing with observations (for a recent review, see Brunetti 2002).

Coma C in the Coma cluster is the prototype of radio halos in galaxy clusters. Being the best studied example, Coma C has been observed at many different radio wavebands (e.g., Schlickeiser, Sievers, & Thiemann 1987; Kim et al. 1990; Venturi, Giovannini, & Feretti 1990; Giovannini et al. 1993; Deiss et al. 1997; Thierbach, Klein, & Wielebinski 2003). Deiss et al. (1997) argued that the measurement at 2.7 GHz by Schlickeiser et al. (1987) is too low and suggested that the integrated spectrum might have no tendency to steepen as suggested by Schlickeiser et al. (1987); however, this strong steepening of the radio spectrum at high frequencies was confirmed by Thierbach et al. (2003). Giovannini et al. (1993) used the radio data at 1380 MHz (Kim et al. 1990) and 326 MHz (Venturi et al. 1990) to derive the radial distribution of the spectral index in Coma C, and they found a central “plateau” with a size of  $\sim 15'$  for the spectral-index distribution. In the central region, the value of the spectral index is  $\sim 0.8$ ; in the outside region, the spectral index strongly steepens as the radius increases.

Observations with *BeppoSAX* and the *Rossi X-ray Timing Explorer (RXTE)* have detected a hard X-ray (HXR) excess with respect to thermal emission from the Coma cluster (Fusco-Femiano et al. 1999; Rephaeli, Gruber, & Blanco 1999; Rephaeli & Gruber 2002). The HXR excesses from several other clusters have also been reported (Kaastra et al. 1999; Fusco-Femiano et al. 2000, 2001; Gruber & Rephaeli 2002). The most favored mechanism of the HXR excess is inverse Compton scattering (ICS) of the cosmic microwave background (CMB) photons by relativistic electrons. Since these electrons with energy  $\gamma \sim 10^4$  will also produce radio synchrotron radiation, the HXR excesses and radio halos may originate from the same electron population. In the Coma cluster, the volume-averaged values of magnetic fields deduced from the comparison of the radio with the HXR excess emission is  $\sim 0.1\text{--}0.3 \mu\text{G}$  (Fusco-Femiano et al. 1999; Rephaeli et al. 1999; Rephaeli & Gruber 2002). These low values of field strength are not consistent with those deduced from the measurements of Faraday rotation. Clarke, Kronberg, & Böhringer (2001) have shown that many clusters have relatively large ( $\sim 4\text{--}8 \mu\text{G}$ ) fields. For the Coma cluster, Kim et al. (1990) found a central field strength of  $1.7 \pm 0.9 \mu\text{G}$ , and Feretti et al. (1995) estimated the strength to be  $6 \pm 1 \mu\text{G}$ . It is thus very important to see whether it is possible to produce the observed

HXR excess via the inverse Compton mechanism with such a high central magnetic field. Nonetheless, some uncertainties in both methods may lead to the discrepancy (Newman, Newman, & Rephaeli 2002). An alternative interpretation of the HXR excess is non-thermal bremsstrahlung from supra-thermal electrons (Enßlin, Lieu, & Biermann 1999; Blasi 2000; Dogiel 2000; Sarazin & Kempner 2000). However, a huge amount of energy is necessary in this model to produce the observed HXR excess (Petrosian 2001; Blasi 2000).

Brunetti et al. (2001) proposed a two-phase model to interpret the radial steepening of the spectral-index distribution in Coma C. In this two-phase model, the relativistic electrons were injected during a first phase in the past and re-accelerated during a second phase up to present time. In such a re-acceleration model, there must be a cutoff in the electron spectrum because of the balance between the loss and the gain of the electron energy. A cutoff in the electron spectrum should lead to a cutoff in the emissivity of synchrotron radiation and then in the integrated radio spectrum. If the magnetic fields have a radial-decrease profile, the cutoff frequencies will decrease with the increasing radius. Consequently, a radial steepening of the spectral index between two fixed frequencies will appear. Brunetti et al. (2001) successfully reproduced the radial steepening of the spectral index, the radio spectrum steepening at high frequencies, and the HXR excess in the Coma cluster; however, the central “plateau” in the spectral-index distribution was not well explained. The authors adopted a central field strength of  $\lesssim 3 \mu\text{G}$  in their models. As pointed in their work, the spectral index would be very steep in low magnetic fields and flat in moderate ones. It would be important to know whether a stronger central magnetic field can reproduce the central “plateau” in the spectral-index distribution without violating the observational constraints from the radio and HXR emission.

Cluster mergers are very violent events and release a large amount of energy ( $\sim 10^{64}$  ergs). Merger shocks and violent turbulence must play an important role in the generation and re-acceleration of relativistic electrons (Sarazin 2001). Nonetheless, Gabici & Blasi (2003) claimed that the shocks generated by major mergers, mergers between clusters with comparable mass, is too weak to account for the spectral slopes of the non-thermal emission. The Mach numbers of the shocks in major mergers are of order of unity in their simulations and roughly consistent with the Mach number  $\sim 2$  observed in Cygnus A (Markevitch, Sarazin, & Vikhlinin 1999). However, if a significant level of re-acceleration is involved, the evolved spectra of relativistic electrons may be able to account for the observed spectra of non-thermal emission.

In this paper, we investigate the radio and HXR excess emission in the Coma cluster assuming the magnetic fields possessing a central field strength of  $6 \mu\text{G}$  and a radial-decrease profile. The effects of different Mach numbers of merger shocks on the formation of radio

halos and HXR excesses are also investigated. We assume that relativistic electrons are injected by merger shocks and re-accelerated by ensuing violent turbulence. The turbulence is expected to be more violent at the moment right after the merger shocks and then gradually decays with time (Ricker & Sarazin 2001); therefore, particles in the ICM might obtain stronger re-acceleration in the early period of mergers and then, following the decay of turbulence, the strength of re-acceleration would decrease. In this work, both time-independent and time-dependent re-acceleration models are considered. The radial variation of the spectral index of synchrotron radiation in the Coma cluster is computed to test the scenarios of the cosmic-ray electron re-acceleration. In particular, we try to obtain a central “plateau” in the spectral-index distribution that is in agreement with observational results reported by Giovannini et al. (1993). We also investigate the production of an HXR excess with the assumption that the HXR excess is due to ICS of the CMB photons by the cosmic-ray electron distribution that we obtained from the spectral index fitting. Comparing the modelling results with the observations, we find that the Mach numbers of the merger shocks have to be in a very small range to form the radio halo and the HXR excess observed in the Coma cluster.

In this paper,  $H_0 = 50 \text{ km s}^{-1} \text{ Mpc}^{-1}$  is assumed. The red shift  $z$  of the Coma cluster is  $\sim 0.0233$ , so that the distance is  $\sim 140 \text{ Mpc}$  and  $1'$  corresponds to  $\sim 40 \text{ kpc}$ . The virial radius of  $3.28 \text{ Mpc}$  (Girardi et al. 1998) is adopted as the radius of the Coma cluster.

## 2. PARTICLE ACCELERATION MODELS

The energy variation of particles can be expressed as:

$$-\frac{d\gamma}{dt} = b_0 + b_1\gamma + b_2\gamma^2, \quad (1)$$

where  $b_0 = b_{\text{Coul}}$ ,  $b_1 = b_{\text{brem}} - b_{\text{acc}}$ , and  $b_2 = b_{\text{syn}} + b_{\text{IC}}$ . The coefficients of the loss rates due to the Coulomb and bremsstrahlung losses can be approximated as (Sarazin 1999):

$$b_{\text{Coul}} \approx 1.2 \times 10^{-12} n_{\text{gas}} \left[ 1.0 + \frac{\ln(\gamma/n_{\text{gas}})}{75} \right] \text{ s}^{-1},$$

and

$$b_{\text{brem}} \approx 1.51 \times 10^{-16} n_{\text{gas}} [\ln(\gamma) + 0.36] \text{ s}^{-1},$$

where  $n_{\text{gas}}$  is the gas density. For the Coma cluster, it can be defined as:

$$n_{\text{gas}}(r) = n_0 f_{\text{gas}}(r) = n_0 \left[ 1 + \left( \frac{r}{r_{\text{gas}}} \right)^2 \right]^{-3\beta_{\text{gas}}/2}, \quad (2)$$

where  $n_0 = 2.89 \times 10^{-3} \text{ cm}^{-3}$ ,  $r_{gas} = 10'5 \approx 0.42 \text{ Mpc}$ , and  $\beta_{gas} = 0.75$  (Briel, Henry, & Böhringer 1992). We set  $\gamma = 10^3$  and  $n_{gas} = 10^{-3} \text{ cm}^{-3}$  into the logarithms for simplicity.

The coefficients in the loss function of inverse Compton scattering and synchrotron radiation can be expressed as (Sarazin 1999):

$$b_{IC} = 1.37 \times 10^{-20} (1+z)^4 \text{ s}^{-1},$$

and

$$b_{syn} = 1.3 \times 10^{-21} \left( \frac{B}{1 \mu G} \right)^2 \text{ s}^{-1},$$

where  $z \ll 1$  is assumed in these calculations.

To account for the temporal dependence of the electron re-acceleration due to violent turbulence, the general form of the acceleration function  $b_{acc}$  is given by:

$$b_{acc}(r, t) = b_a(r)g(t), \quad (3)$$

where

$$b_a(r) = a_0 + a_1 f_a(r) \quad (4)$$

$$g(t) = 1 + Ae^{-Dt}. \quad (5)$$

The parameters  $A$  and  $D$  are the amplification factor and the dissipation factor, respectively. The cases with  $A = D = 0$  are called time-independent acceleration, and the cases with  $A \neq 0$  and  $D \neq 0$  are called time-dependent acceleration. According to the numerical work of Ricker & Sarazin (2001), the maximum temperature of mergers is  $\lesssim$  three times of the initial temperature before merging and returns to that when the passed times after merging are greater than 1 Gyr. Because the sources for heating gas are turbulence and shocks generated by merging, it is reasonable to relate the temperature variation with the turbulence strength, i.e., the strength of re-acceleration. Thus we choose the values of the amplification factor  $A$  and the dissipation factor  $D$  under the constraint that the maximum value of  $g(t)$ , i.e.,  $1 + A$ , is  $\lesssim 3$  and the value of  $g(t)$  is  $\sim 1$  when  $t = 1 \text{ Gyr}$  in our models.

The re-acceleration model in the two-phase model proposed by Brunetti et al. (2001) is a time-independent acceleration model in our classification. Brunetti et al. (2001) suggested that the re-acceleration function ( $\chi(r)$  in their eq. [16] corresponding to  $b_a(r)$  here) can be parameterized as the sum of a uniform large-scale component and a small-scale component and assumed that the uniform large-scale component is caused by shocks and/or turbulence, possibly generated during a recent merger, and the small-scale component assumed to be proportional to the inverse of the typical distance between galaxies is due to the amplification of these shocks/turbulence by the motion of the massive galaxies in the cluster core. Following

Brunetti et al. (2001), we assume that the acceleration component  $a_0$  in the re-acceleration function  $b_a(r)$  is due to turbulence and spatially uniform in the cluster. The lower-hybrid-wave turbulence proposed by Eilek & Weatherall (1999) is a possible scenario for this kind of re-acceleration. They showed that large amplitude Alfvén waves do generate lower hybrid waves which collapse to produce localized, intense wave packets, and even a modest level of lower hybrid turbulence can be very effective at accelerating relativistic particles. For the  $a_1 f_a(r)$  component (corresponding to the small-scale component in the two-phase model), we assume that this is caused by the orbiting motion of galaxies. According to the work of Deiss & Just (1996), the excited turbulent motions of ICM are related to the galaxy density in the cluster and vary as  $v_{turb}^2 \propto n_{gal}$ , so that we assume  $f_a(r) \propto n_{gal}$ . The  $\beta$ -model is adopted for the galaxy distribution in the Coma cluster:

$$n_{gal}(r) \propto f_{gal}(r) = \left[1 + \left(\frac{r}{r_{gal}}\right)^2\right]^{-3\beta_{gal}/2}, \quad (6)$$

where  $r_{gal} \approx 0.18$  Mpc and  $\beta_{gal} = 0.86$  (Girardi et al. 1998). We define  $f_a(r) = f_{gal}(r)$ .

For time-independent acceleration, the analytic solution of equation (1) with the condition that  $\gamma$  and  $n_{gas}$  are constant in the logarithms of the Coulomb and bremsstrahlung losses are (see, e.g., Brunetti et al. (2001)):

$$\tau = \frac{2}{\sqrt{|\eta|}} (\tanh^{-1} y - \tanh^{-1} y_0), \quad (7)$$

where

$$\begin{aligned} \tau &= t - t_0, \\ \eta &= 4b_0b_2 - b_1^2, \\ y &= \frac{2b_2\gamma + b_1}{\sqrt{|\eta|}}, \\ y_0 &= \frac{2b_2\gamma_0 + b_1}{\sqrt{|\eta|}}. \end{aligned}$$

The notation  $\gamma_0$  is the energy of electrons at time  $t_0$ .

This solution can be rewritten as:

$$\gamma(t) = \frac{\sqrt{|\eta|}}{2b_2} \left( \frac{y_0 + \tanh x}{1 + y_0 \tanh x} \right) - \frac{b_1}{2b_2}, \quad (8)$$

where

$$x = \frac{\sqrt{|\eta|}}{2} \tau.$$

The cutoff energy is defined by setting  $\gamma_0 = \infty$  at time  $t_0$  in equation (8) and can be expressed as:

$$\gamma_c(t) = \frac{\sqrt{|\eta|}}{2b_2 \tanh x} - \frac{b_1}{2b_2}. \quad (9)$$

### 3. INJECTION AND EVOLUTION OF THE ELECTRON SPECTRUM

In our models, the relativistic electrons are assumed to be injected by merger shocks. A power-law spectrum of relativistic electrons is expected from diffuse shock acceleration. We assume that the injected spectrum has the form:

$$n_e(\gamma, r) = f_e(r) K_e \gamma^{-s}, \quad (10)$$

where  $f_e(r)$  is assumed to be proportional to the gas distribution and is normalized to be equal to  $f_{gas}(r)$  as described in equation (2), i.e.,  $f_e(r) = f_{gas}(r)$ . The parameter  $K_e$  can be determined by normalizing the theoretical radio spectrum to the observed data. The power-law index  $s$  is related to the Mach number  $\mathcal{M}$  of the merger shocks by the expression:  $s = 2(\mathcal{M}^2 + 1)/(\mathcal{M}^2 - 1)$  (e.g., Gabici & Blasi 2003). For studying the effects of the Mach numbers of merger shocks on the non-thermal emission in galaxy clusters, we adopt different values for the power-law index  $s$ : 2.5, 3.3, 4.0, and 4.7 corresponding to Mach numbers: 3, 2, 1.73, and 1.58, respectively. Without loss of generality, we ignore the initial variation of the power-law index in the cluster for simplicity.

Cosmic-ray protons can also generate secondary electrons. Nonetheless, it is still unclear about the contribution of the secondary electrons to the relativistic electrons in galaxy clusters. In our calculation, we consider only the electrons injected by merger shocks, and assume that the secondary electrons are negligible (Kuo, Hwang, & Ip 2003).

The evolution of the electron population is described by the kinetic equation:

$$\frac{\partial n_e(\gamma)}{\partial t} = \frac{\partial}{\partial \gamma} [b(\gamma) n_e(\gamma)] + q(\gamma), \quad (11)$$

where  $b(\gamma) = b_0 + b_1 \gamma + b_2 \gamma^2$ . Here we assume no continuous injections, i.e.,  $q(\gamma) = 0$ . The analytic solution of equation (11) for time-independent acceleration is then:

$$n_e(\gamma, t) = n_e(\gamma_0, t_0) \left[ \frac{1 - \tanh^2 x}{(1 - y \tanh x)^2} \right], \quad (12)$$

where  $x$  and  $y$  are defined in equations (8) and (7), respectively.

#### 4. DISTRIBUTION OF MAGNETIC FIELDS IN COMA

Using the techniques of dimensional analysis for studying turbulent structures, Jaffe (1980) derived a magnetic field model determining by the gas and galaxy distributions and described by:

$$B(r) = B_0 f_B(r) = B_0 [f_{gas}(r)]^m [f_{gal}(r)]^n, \quad (13)$$

where  $f_{gas}(r)$  and  $f_{gal}(r)$  are defined in equations (2) and (6), and  $(m, n) = (0.5, 0.4)$ . For the Coma cluster, there are other constraints that can be used to determine the profile of magnetic fields; the observed spectral-index distribution possesses a central “plateau” and strongly steepens outside this region. It is expected that the profile of the magnetic field strongly affected the size of the central “plateau” and the steepness of the spectral-index distribution outside this region. We assume the central field strength  $B_0$  is  $6 \mu\text{G}$ . The profile with  $(m, n) = (0.7, 0.3)$  shown in Figure 1 is chosen in our paper in order to make the size of the central “plateau” and the steepness of the spectral-index distribution outside this region calculated in the acceleration models agreeing with the observations.

The orbiting motion of galaxies might amplify the seed fields to grow into the present magnetic field in galaxy clusters (Jaffe 1980; Roland 1981; Ruzmaikin, Sokoloff, & Shukurov 1989). However, De Young (1992) has shown that the turbulent dynamo driven by the galaxy motion is difficult to produce the present micro-gauss fields. Cluster merging, a very energetic process, may offer a possibility to produce the observed fields. Because the decay time of the magnetic field is very long, the magnetic field will gradually build up under successive merging (Tribble 1993). It is reasonable to assume that the observed fields at the present time is the amplified fields after the last merging. This is the reason for the assumption that the magnetic field is time-invariant in our models.

We note that the profile of  $(m, n) = (0.7, 0.3)$  is adopted for the purpose of reproducing the observed spectral-index distribution and might be different from a real distribution of cluster magnetic fields. For examples, the profiles of simulated magnetic fields are flat in the core region and the fields are  $\sim 1 \mu\text{G}$  (Dolag, Bartelmann, & Lesch 2002). From the Faraday rotation measurements, the magnetic fields are  $\sim 4\text{--}8 \mu\text{G}$  out to  $\sim 0.75 \text{ Mpc}$  from cluster centers (Clarke et al. 2001). The adopted central magnetic field is higher than the simulated results but lower than the observational ones.

#### 5. MODELLING PROCEDURE

In this section, we briefly describe the methods for calculations. We assume the electron spectra have a power law at time  $t = 0$ , which corresponds to the moment right after the



main-merger shock. The electron spectra have an initial power-law index  $s$  according to the Mach number of the shock and would then evolve according to the formulism described in § 2 and § 3. Since a flat central region in the spectral-index distributions of the radio-halo emission may exist only in a short period during the evolution of radio halos, we calculate the brightness distributions at two fixed frequencies, 326 MHz and 1380 MHz, for different evolution time scales and derive the spectral-index distribution from them. To fit and compare our models with observations, we first vary the acceleration function  $b_{\text{acc}}(r, t)$  and judge whether the corresponding spectral-index distributions are consistent with the observations according to two criteria: (1) there is a flat central region with  $\alpha_{326}^{1380} = 0.8$  as reported by Giovannini et al. (1993) and (2)  $\alpha_{326}^{1380} = 1.8$  is located in the range of  $16'–18'$  to agree with the results obtained by Deiss et al. (1997). The spectral-index distributions at different time  $t$  with a step of 0.2 Gyr are computed until consistency with the criteria have been obtained. Second, we also calculate the spatial brightness distributions at 326 MHz to compare with the observed one at 90 cm (Govoni et al. 2001, kindly provided by F. Govoni). Third, we normalize the theoretical radio spectrum to the observed data at 430 MHz and then determine the normalized parameter  $K_e$  in equation (10). Finally, the HXR spectrum is calculated in a region with a projected radius of  $50'$  and compared with the observational data from *BeppoSAX* (Fusco-Femiano et al. 1999) and *OSSE* (Rephaeli, Ulmer, & Gruber 1994). The thermal temperature of the cluster is assumed to be 8.21 keV (Hughes et. al. 1993) in our calculations.

## 6. MODEL RESULTS FOR COMA C

### 6.1. Time-Independent Re-Acceleration

We study the time-independent re-acceleration models by assuming that the amplification and dissipation factors in the acceleration function are zero. Different initial power-law indices corresponding to different Mach numbers are considered. The values of the parameters in the time-independent models are listed in Table 1.

Figure 2 shows the results from the models with the power-law index  $s = 2.5$  (models A1 and A2). The radii of the flat central regions in the spectral-index distributions are  $\approx 6'$  in both models, which is roughly in consistent with the observations. Nonetheless, the spatial brightness distributions are much more concentrated toward the central regions comparing with observations; the integrated radio spectra also deviate from the measured data both at the low and high frequency parts. The HXR spectra are too low to compare with the observations. These results show that a merger shock with a Mach number  $\mathcal{M} \approx 3$  cannot produce the radio and HXR emission observed in the Coma cluster.

Figure 3 and Figure 4 show the results with the power-law index  $s = 3.3$  (models A3 and A4) and the power-law index  $s = 4$  (models A5 and A6), respectively. All these models can produce a flat spectral-index distribution with a radius of  $\approx 5'–6'$  in the central regions. The brightness distributions and the HXR spectra are all roughly consistent with the observations in these models, although distributions seem to be better described by the  $s = 4$  models than the  $s = 3.3$  ones. These models can also match the integrated radio spectra very well; the spectra also seem to be better fitted by the models with  $s = 4$  than those with  $s = 3.3$ . These results indicate that merger shocks with Mach numbers  $\mathcal{M} \lesssim 2$  can produce the main features of the radio and HXR emission observed in the Coma cluster.

Figure 5 shows the results with the power-law index  $s = 4.7$  (models A7 and A8). We cannot obtain the spectral-index distributions that have a spectral index  $\alpha_{326}^{1380} = 1.8$  in the region  $16'–18'$  that satisfy the second criterion described in § 5 for models with a power-law index  $s = 4.7$  or higher when we fit the central flat spectral index to  $\alpha_{326}^{1380} \approx 0.8$ . Nonetheless, we try to find a flat central distribution in the spectral index distribution for these models by ignoring the second criterion. The results are shown in Figure 5. The radii of the flat central regions are  $\approx 4'$  in model A7 and  $\approx 6'$  in model A8. The spectral index  $\alpha_{326}^{1380} = 1.8$  locates at radius larger than  $20'$  in both models. The spatial brightness distributions show a flat distribution in the central regions; this is particularly obvious for models A8. Both models do not fit the integrated radio spectral data at high frequencies; model A8 also overproduces the HXR excess. These results indicate that it is difficult to produce all observed features of the radio and HXR emission in the Coma cluster by mergers shocks with Mach numbers  $\mathcal{M} \leq 1.6$ .

According to the results shown in Figures 2–5, a central “plateau” in the spectral-index distribution can be produced for all these models. Nonetheless, only the models with the initial electron power-law index  $4.7 > s \gtrsim 3.3$  can produce results that match all observed features of the radio and HXR emission in the Coma cluster; this corresponds to a very narrow range for the Mach numbers of the merger shocks, i.e.,  $1.6 < \mathcal{M} \lesssim 2$ .

## 6.2. Time-Dependent Re-Acceleration

In this section, we show the effects of time-dependent re-acceleration by assuming that the amplification factor  $A = 1$  and the dissipation factor  $D = 2 \text{ Gyr}^{-1}$ . We note that the values of  $A$  and  $D$  are constrained by the conditions  $1 + A \lesssim 3$  and  $Ae^{-Dt}$  becoming sufficient small as  $t$  approaching 1 Gyr. Since we just want to investigate the effects of the time-dependent re-acceleration on our current models, we fix the values of  $A$  and  $D$  for simplicity. A suitable but different choice of  $A$  and  $D$  could affect the results, particularly,

on the evolving time scales that fit the observations. The values of the parameters in the time-dependent models are listed in Table 2. Since the results from the time-independent models with  $s = 2.5$  and  $4.7$  strongly deviate from the observations, we consider only the cases of  $s = 3.3$  and  $4$  in the time-dependent models.

Figure 6 shows the results with the power-law index  $s = 3.3$  (models B1 and B2). The flat central regions in the spectral-index distributions have radii of  $\approx 6'$  in both models B1 and B2. However, we note that in the model B2 the spectral index  $\alpha_{326}^{1380} = 1.8$  locates at  $\approx 20'$ , which does not satisfy the second criterion stated in § 5. The brightness distributions are concentrated to the central regions resembling those from models A1 and A2. These results indicate that models with time-dependent re-acceleration have effects similar to those with flatter initial electron spectra. This also shows that merger shocks with Mach numbers,  $\mathcal{M} \geq 2$ , i.e.,  $s \leq 3.3$ , cannot produce the radio emission observed in the Coma cluster.

Figure 7 shows the results with the power-law index  $s = 4$  (models B3 and B4). The flat central regions in the spectral-index distributions have a radius of  $\approx 4'$  in model B3 and  $\approx 6'$  in model B4. The integrated radio spectra and the HXR spectra obtained from both models are all in very good agreement with the observations. The brightness distributions also agree very well with the observations in inner part of the cluster, but are slightly lower than the observed ones at the radii greater than  $18'$ .

We find that the radio spatial brightness distribution is very sensitive in these time-dependent models. Our results indicate that the models with time-dependent re-acceleration have effects on the brightness distribution similar to those with flatter initial electron spectra. These effects can be understood because the time-dependent re-acceleration function provides a larger re-acceleration to the electrons at the early stage of the evolution; this is similar to have a flatter initial electron spectrum. Nonetheless, time-dependent models can still fit the integrated radio spectra and the HXR excess emission better. Combining the results from the time-independent and time-dependent models, we find that only merger shocks with Mach numbers,  $1.6 < \mathcal{M} < 2$ , i.e., the power-law index  $4.7 > s > 3.3$ , can reproduce the results agreeing with the observations in the Coma cluster.

## 7. DISCUSSION

As shown in the modelling results, a central “plateau” in the spectral-index distribution can be produced in clusters with a central field strength of  $6 \mu\text{G}$ . To understand the origin of this characteristic feature of the radio emission of Coma C, we use the results of Model A6 as an example and show the electron spectra and the radio emissivity of this model at

different locations in Figures 8 and 9, respectively. It is obvious that the electrons in the central regions are strongly accelerated to the cutoff energies and flat spectra can be formed within the central  $10'$  regions. The ratios between the radio emissivity at 326 MHz and that at 1380 MHz are almost equal within the central regions and, at these two frequencies, the radio emissivity within the central regions dominates over that outside this regions; thus a central “plateau” may form in the spectral-index distribution. Outside the central region, the electron spectra are not very different from one another because the effects are mainly from the inverse Compton losses and the spatially uniform re-acceleration, and then the differences between the radio emissivity at different locations are mainly due to the variations of the magnetic fields. As the radius increases, the high-frequency emissivity gradually decreases because of weaker magnetic fields; therefore, the progressive steepening of the spectral index is presented. Naturally, it should also exist a decline at high frequencies in the integrated radio spectrum as proposed by Schlickeiser et al. (1987).

It is interesting to note that the size of the “plateau” is almost equal to the region where the magnetic field is  $\gtrsim 3 \mu\text{G}$  (Figure 1). This fact might indicate that the formation of this “plateau” is related to the situation that the synchrotron losses dominate over the inverse Compton losses (e.g., Brunetti et al. 2001). The “plateau” should be produced by the combination of the radial setting of re-acceleration and that of magnetic fields. As discussed in previous paragraph, when the inverse Compton losses dominate, it is impossible to obtain a flat “plateau” because the radius-dependent magnetic fields will cause the high-frequency emissivity to decrease as the radius increase. In other words, it is possible to obtain a flat spectral index “plateau” in our models only when the synchrotron losses dominate over the inverse Compton losses. If a central “plateau” presents in the spectral-index distribution, the central strength of the cluster magnetic field should be greater than  $3 \mu\text{G}$ . Note that since a central “plateau” can exist only in a period in the evolution of radio halos, a central “plateau” in the spectral-index distribution may be absent even a cluster possessing a high central field.

The emissivity of the HXR excess of the Model A6 is shown in Figure 10. Obviously, the HXR excess is mainly contributed from the outer regions of the cluster volume ( $> 30'$ ) as indicated by Brunetti et al. (2001). This might reconcile the problem that the volume-averaged magnetic fields derived from the HXR excesses are usually much lower than the magnetic fields from the Faraday rotation measurements. However, we note that the average magnetic field in the core regions adopted here is  $\lesssim 2 \mu\text{G}$  while the magnetic fields from the Faraday rotation measurements are  $\approx 6 \mu\text{G}$ . It might be possible that a further fine-tuned version of our model can solve the problem of the high field–ICS discrepancy.

It is expected that the profile and strength of magnetic fields will affect our results. From

the Faraday rotation measurements, the magnetic fields are  $\sim 4\text{--}8 \mu\text{G}$  out to  $\sim 0.75 \text{ Mpc}$  from cluster centers (Clarke et al. 2001). We note that the magnetic fields in galaxy clusters might have a higher value and a flatter profile in the core region than the adopted model. A higher magnetic field requires a stronger re-acceleration to sustain the radio emission. To produce a “plateau” distribution of the spectral index for a higher magnetic field with a flatter profile, the re-acceleration function need to be almost constant over the region. This indicates that the re-acceleration caused by the galaxy motions might be negligible.

The ICS of the CMB photons by relativistic electrons is also suggested as the mechanism of the extreme-ultraviolet (EUV) excess in the Coma cluster (Hwang 1997; Enßlin, & Biermann 1998). However, the EUV excess possesses a narrow radial profile and concentrates in the inner regions of the cluster (Bowyer & Berghöfer 1998), while the HXR excess is mainly contributed from the outer regions of the cluster volume as shown in Figure 9. It is thus inadequate to assume that the EUV-emitting electrons are also from the outside and low-magnetic-field regions of the cluster. Tsay, Hwang, & Bowyer (2002) investigated the EUV excess with a  $\sim 5 \mu\text{G}$  field; they showed that it is possible to explain the EUV excess and the radio emission with such a high average magnetic field. The EUV-emitting electrons and the radio/HXR-emitting electrons could have very different distributions because the low-energy EUV-emitting electrons suffer much less energy losses during their evolution and can accumulate over a much longer age.

## 8. SUMMARY

Time-independent and time-dependent re-acceleration models are studied to investigate the formation of the radio halo and HXR excess in the Coma cluster with a high central field strength of  $6 \mu\text{G}$ . In these models, the relativistic electrons are injected by merger shocks and re-accelerated by ensuing violent turbulence. The effects of the strength of merger shocks on the formation of the radio halo and HXR excess are also considered.

We have reproduced all the main features in the radio and HXR excess emission of the Coma cluster in our models. We have obtained a central “plateau” in the spectral-index distribution as observed in the Coma cluster with a high central field strength of  $6 \mu\text{G}$  in our models. The size of the “plateau” is almost equal to the region where the synchrotron loss dominates over the inverse Compton loss, i.e., the magnetic field is  $\gtrsim 3 \mu\text{G}$ . Our models can naturally produce the observed radial steepening of the radio spectral index. We can fit the integrated radio spectra very well, in particular, we can reproduce the high-frequency decline feature in the spectra as measured by Thierbach et al. (2003). These same models can also produce the observed HXR excess, which is mainly from the outer regions of the

cluster volume as pointed out by Brunetti et al. (2001).

We have also shown that only merger shocks with Mach numbers in a very small range can produce results agreeing with the observations of the radio and HXR emission in the Coma cluster. The Mach numbers are  $1.6 < \mathcal{M} < 2$ , corresponding to the initial electron power-law index  $4.7 > s > 3.3$ , which are consistent with simulations and observations of merger shocks.

We have adopted an artificial magnetic field distribution in our calculation. The real magnetic field might be higher and have a flatter distribution than the adopted model. It is possible to obtain similar results for a higher magnetic field with a stronger re-acceleration. However, it might have problems to produce the observed HXR excess within the ICS scheme for such a high magnetic field.

We are grateful to S. Bowyer for a careful reading of the manuscript and several suggestions that helped to improve this paper. We thank F. Govoni for kindly providing the data of the Coma radio profile. We are also grateful to an anonymous referee for his valuable comments which stimulated us to significantly improve this paper. This work was partially supported by the National Science Council of Taiwan under NSC 91-2112-M-008-045, and by the Ministry of Education of Taiwan through the CosPA Project 91-N-FA01-1-4-5. CYH acknowledges support by the National Science Council through grant NSC 91-2112-M-008-039.

## REFERENCES

- Blasi, P. 2000, *ApJ*, 532, L9
- Bowyer, S., & Berghöfer, T. W. 1998, *ApJ*, 506, 502
- Briel, U. G., Henry, J. P., & Böhringer, H. 1992, *A&A*, 259, L31
- Brunetti, G., Setti, G., Feretti, L., & Giovannini, G. 2001, *MNRAS*, 320, 365
- Brunetti, G. 2002, in *Matter and Energy in Clusters of Galaxies*, ed. S. Bowyer, & C.-Y. Hwang (San Francisco: ASP), in press (astro-ph/0208074)
- Clarke, T. E., Kronberg, P. P., & Böhringer, H. 2001, *ApJ*, 547, L111
- Deiss, B. M. & Just, A. 1996, *A&A*, 305, 407
- Deiss, B. M., Reich, W., Lesch, H., & Wielebinski, R. 1997, *A&A*, 321, 55
- Dennison, B. 1980, *ApJ*, 239, L93
- De Young, D. S. 1992, *ApJ*, 386, 464
- Dogiel, V. A. 2000, *A&A*, 357, 66
- Dolag, K., Bartelmann, M., & Lesch, H. 2002, *A&A*, 387, 383
- Eilek, J. A. & Weatherall, J. C. 1999, in *Proc. of Ringberg Workshop on Diffuse Thermal and Relativistic Plasma in Galaxy Clusters*, ed. H. Böhringer, L. Feretti, & P. Schuecker (Garching: MPE Rept. 271), 249
- Enßlin, T. A., & Biermann, P. L. 1998, *A&A*, 330, 90
- Enßlin, T. A., Lieu, R., & Biermann, P. L. 1999, *A&A*, 344, 409
- Feretti, L., Dallacasa, D., Giovannini, G., & Tagliani, A. 1995, *A&A*, 302, 680
- Fusco-Femiano, R., Dal Fiume, D., Feretti, L., Giovannini, G., Grandi, P., Matt, G., Molendi, S., & Santangelo, A. 1999, *ApJ*, 513, L21
- Fusco-Femiano, R., et al. 2000, *ApJ*, 534, L7
- Fusco-Femiano, R., Dal Fiume, D., Orlandini, M., Brunetti, G., Feretti, L., Giovannini, G. 2001, *ApJ*, 552, L97
- Gabici, S., & Blasi, P. 2003, *ApJ*, 583, 695

- Giovannini, G., Feretti, L., Ventrucci, T., Kim, K.-T., & Kronberg, P. P. 1993, *ApJ*, 406, 399
- Girardi, M., Giuricin, G., Mardirossian, F., Mezzetti, M., & Boschin, W. 1998, *ApJ*, 505, 74
- Govoni, F., Enßlin, T. A., Feretti, L., & Giovannini, G. 2001, *A&A*, 369, 441
- Gruber, D., & Rephaeli, Y. 2002, *ApJ*, 565, 877
- Hughes, J. P., Butcher, J. A., Stewart, G. C., & Tanaka, Y. 1993, *ApJ*, 404, 611
- Hwang, C.-Y. 1997, *Science*, 278, 1917
- Ip, W.-H., & Axford, W. I. 1999, *Astrophys. Space Sci.*, 264, 437
- Jaffe, W. J. 1977, *ApJ*, 212, 1
- Jaffe, W. J. 1980, *ApJ*, 241, 925
- Kaastra, J. S., Lieu, R., Mittaz, J. P. D., Bleeker, J. A. M., Mewe, R., Colafrancesco, S., & Lockman, F. J. 1999, *ApJ*, 519, L119
- Kim, K.-T., Kronberg, P. P., Dewdney, P. E., & Landecker, T. L. 1990, *ApJ*, 355, 29
- Kuo, P.-H., Hwang, C.-Y., & Ip, W.-H. 2003, *ApJ*, submitted
- Markevitch, M., Sarazin, C. L., & Vikhlinin, A. 1999, *ApJ*, 521, 526
- Newman, W., Newman, A., & Rephaeli, Y. 2002, *ApJ*, 575, 755
- Petrosian, V. 2001, *ApJ*, 557, 560
- Rephaeli, Y., Ulmer, M., & Gruber, D. 1994, *ApJ*, 429, 554
- Rephaeli, Y., Gruber, D., & Blanco, P. 1999, *ApJ*, 511, L21
- Rephaeli, Y., & Gruber, D. 2002, *ApJ*, 579, 587
- Ricker, P. M., & Sarazin, C. L. 2001, *ApJ*, 561, 621
- Roland, J. 1981, *A&A*, 93, 407
- Ruzmaikin, A. A., Sokoloff, D., & Shukurov, A. 1989, *MNRAS*, 241, 1
- Sarazin, C. L. 1999, *ApJ*, 520, 529
- Sarazin, C. L., & Kempner, J. C. 2000, *ApJ*, 533, 73



- Sarazin, C. L. 2001, in *Merging Processes in Clusters of Galaxies*, ed. L. Feretti, I. M. Gioia, & G. Giovannini (Dordrecht: Kluwer), 1 (astro-ph/0105418)
- Schlickeiser, R., Sievers, A., & Thiemann, H. 1987, *A&A*, 182, 21
- Thierbach, M., Klein, U., & Wielebinski, R. 2003, *A&A*, 397, 53
- Tribble, P. C. 1993, *MNRAS*, 263, 31
- Tsay, M. Y., Hwang, C.-Y., & Bowyer, S. 2002, *ApJ*, 566, 794
- Venturi, T., Giovannini, G., & Feretti, L. 1990, *AJ*, 99, 1381

Table 1. Time-Independent Re-Acceleration Models

Model	t (Gyr)	$a_0$ ( $10^{-16} \text{ s}^{-1}$ )	$a_1$ ( $10^{-16} \text{ s}^{-1}$ )
$s = 2.5$			
A1	1.6	1.87	1.52
A2	1.8	1.84	1.53
$s = 3.3$			
A3	1.4	2.18	1.23
A4	1.6	2.07	1.35
$s = 4.0$			
A5	0.8	3.40	0.62
A6	1.0	2.88	0.85
$s = 4.7$			
A7	0.4	7.05	0.01
A8	0.6	5.05	0.30

Table 2. Time-Dependent Re-Acceleration Models with  $A = 1$  and  $D = 2 \text{ Gyr}^{-1}$

Model	t (Gyr)	$a_0$ ( $10^{-16} \text{ s}^{-1}$ )	$a_1$ ( $10^{-16} \text{ s}^{-1}$ )
$s = 3.3$			
B1	1.4	1.90	1.26
B2	1.6	2.02	1.16
$s = 4.0$			
B3	0.8	2.46	0.57
B4	1.0	2.23	0.86

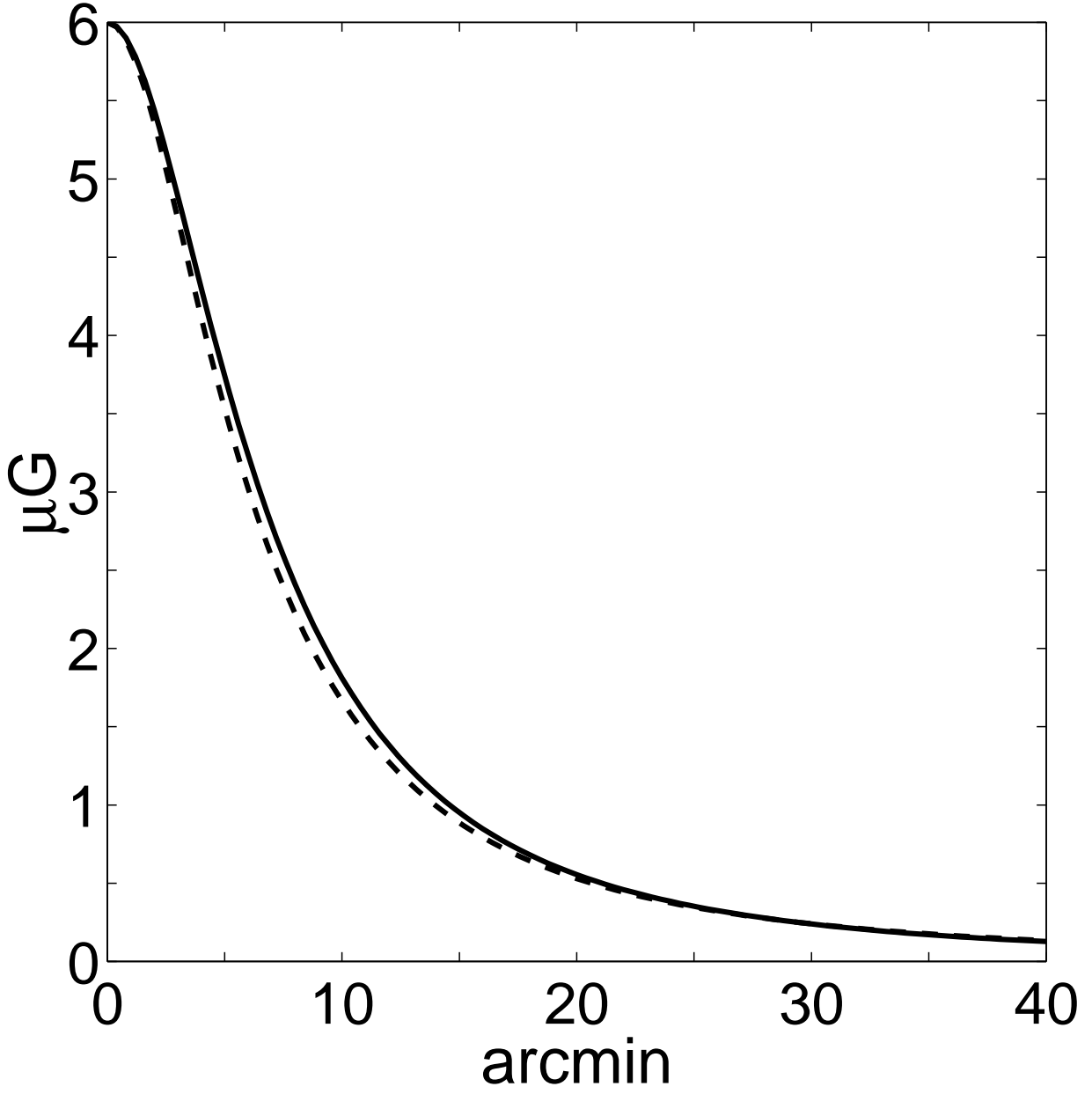


Fig. 1.— Profiles of magnetic fields. The profiles with  $(m, n) = (0.7, 0.3)$  (*solid curve*), and  $(m, n) = (0.5, 0.4)$  (*dashed curve*) are shown. The profile with  $(m, n) = (0.5, 0.4)$  was proposed by Jaffe (1980).

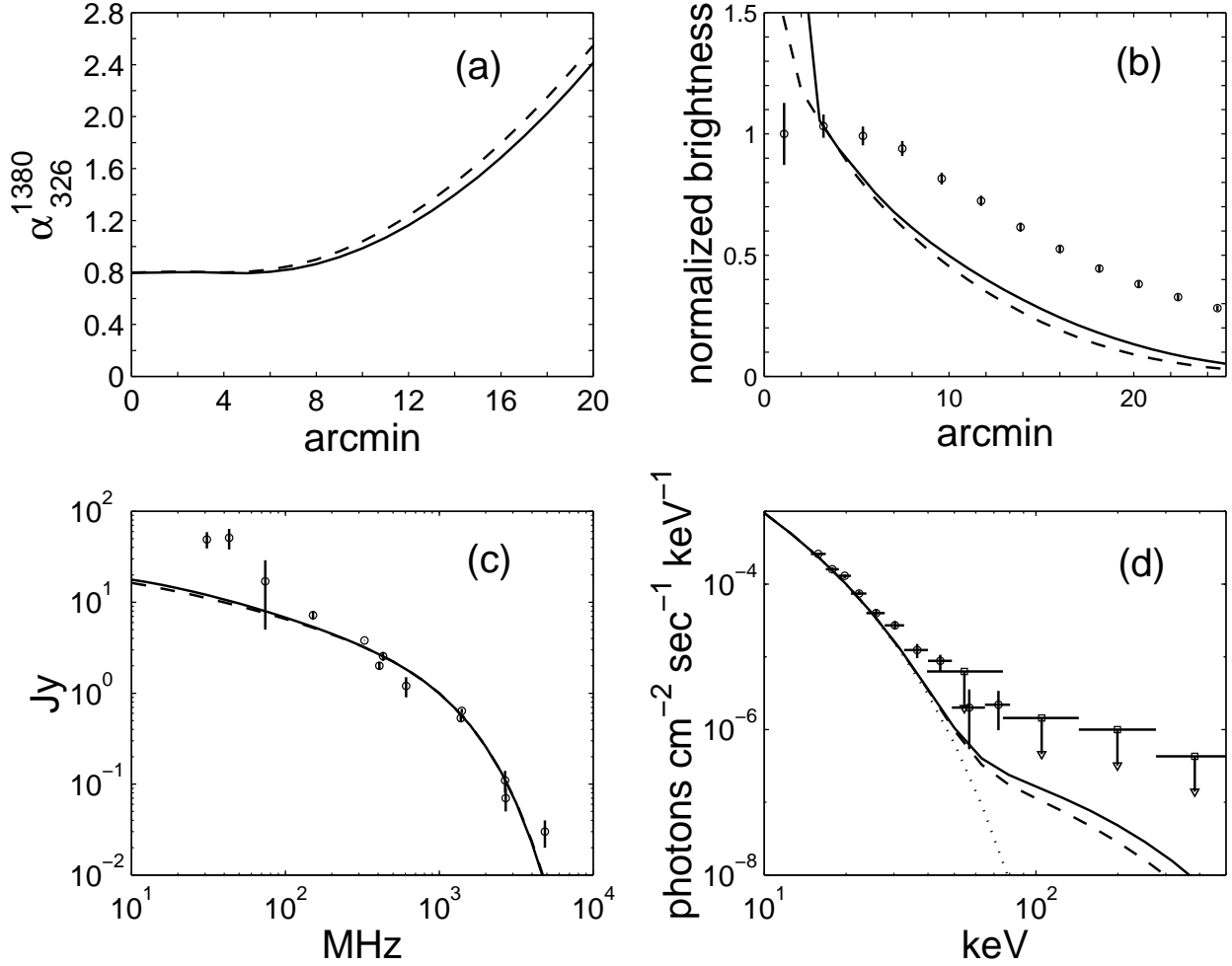


Fig. 2.— Time-independent models with the power-law index  $s = 2.5$ , models A1 (*dashed curve*) and A2 (*solid curve*). (a) Spectral-index distributions. (b) Brightness distributions. The observed brightness is taken from Govoni et al. (2001). (c) Integrated radio spectra. The measured data (*circle*) are taken from Thierbach et al. (2003). (d) HXR spectra. The *dotted curve* is a thermal model with  $kT = 8.21$  keV. The *circle* points are the data from the *BeppoSAX* measurement (Fusco-Femiano et al. 1999) and the *square* points are the upper limits from *OSSE* (Rephaeli et al. 1994).

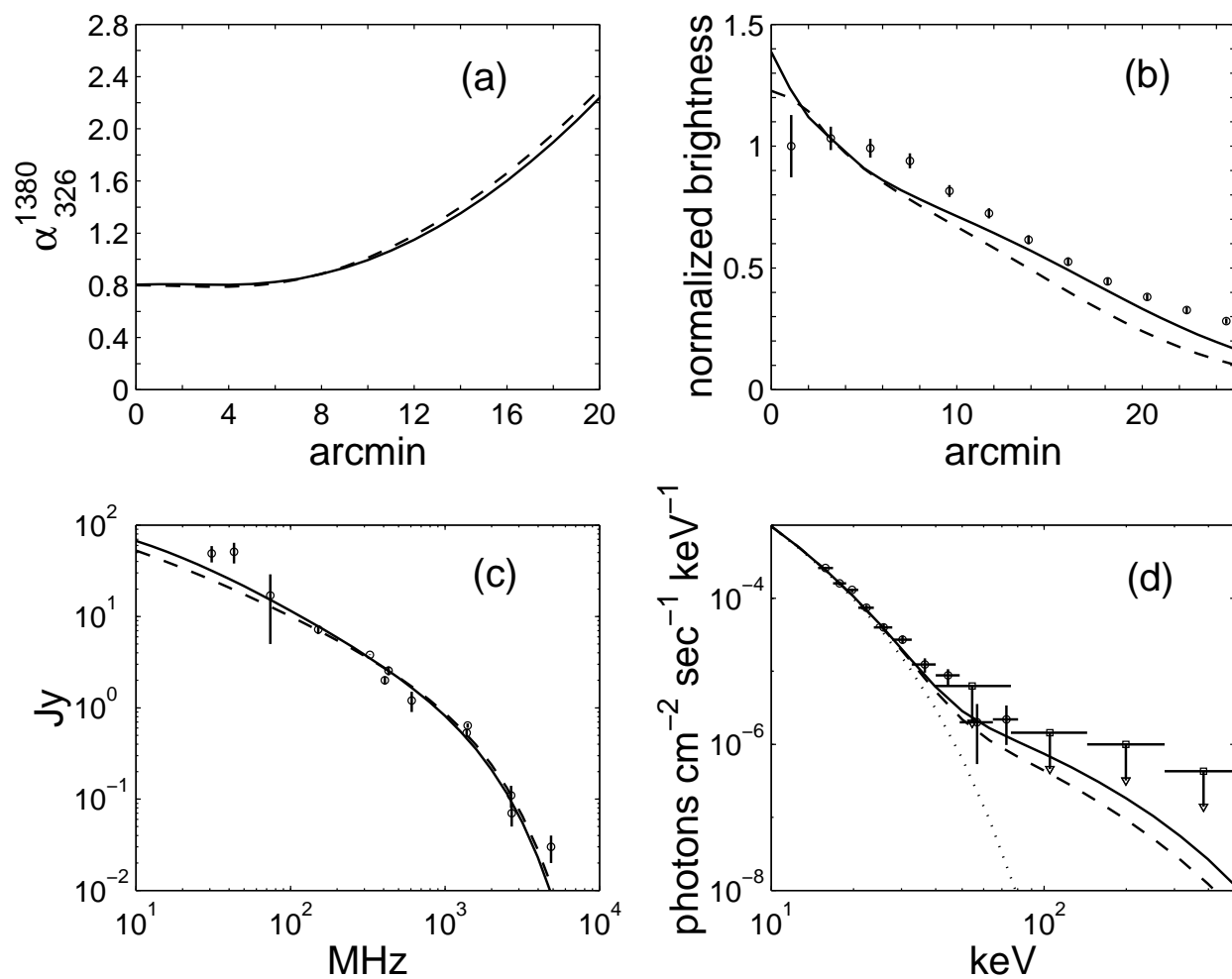


Fig. 3.— Time-independent models with the power-law index  $s = 3.3$ , models A3 (*dashed curve*) and A4 (*solid curve*). (a) Spectral-index distributions. (b) Brightness distributions. (c) Integrated radio spectra. (d) HXR spectra.

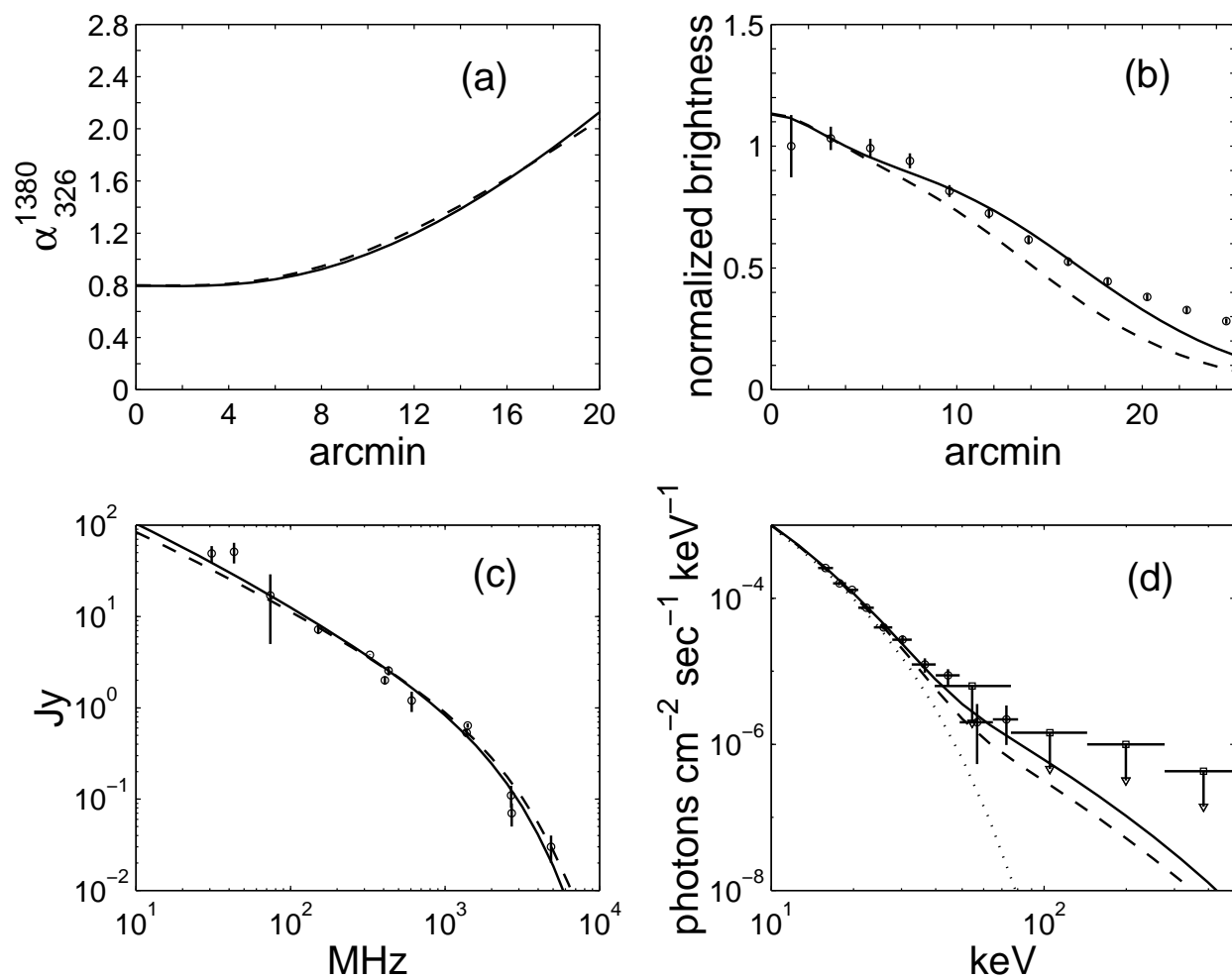


Fig. 4.— Time-independent models with the power-law index  $s = 4.0$ , models A5 (*dashed curve*) and A6 (*solid curve*). (a) Spectral-index distributions. (b) Brightness distributions. (c) Integrated radio spectra. (d) HXR spectra.

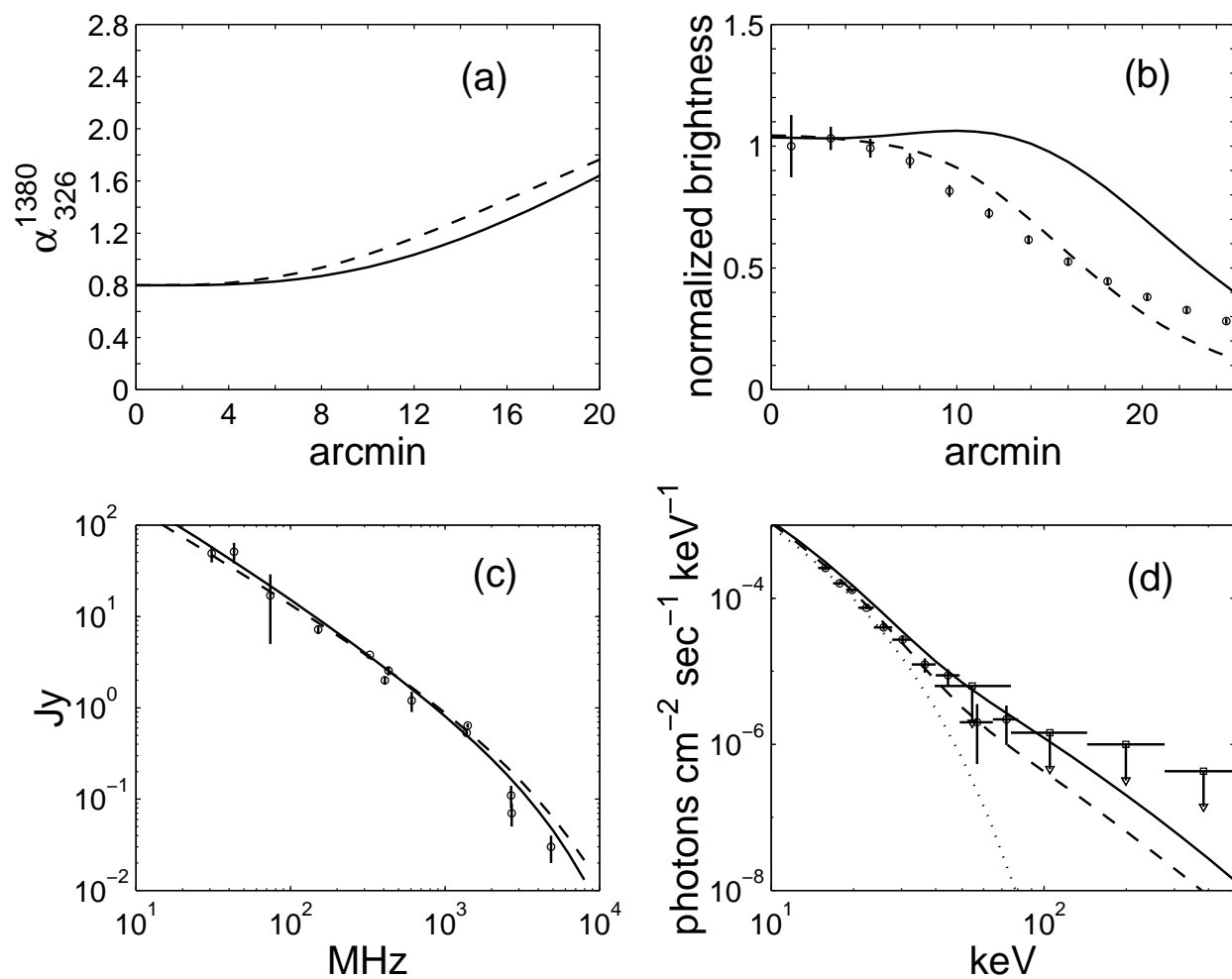


Fig. 5.— Time-independent models with the power-law index  $s = 4.7$ , models A7 (*dashed curve*) and A8 (*solid curve*). (a) Spectral-index distributions. (b) Brightness distributions. (c) Integrated radio spectra. (d) HXR spectra.



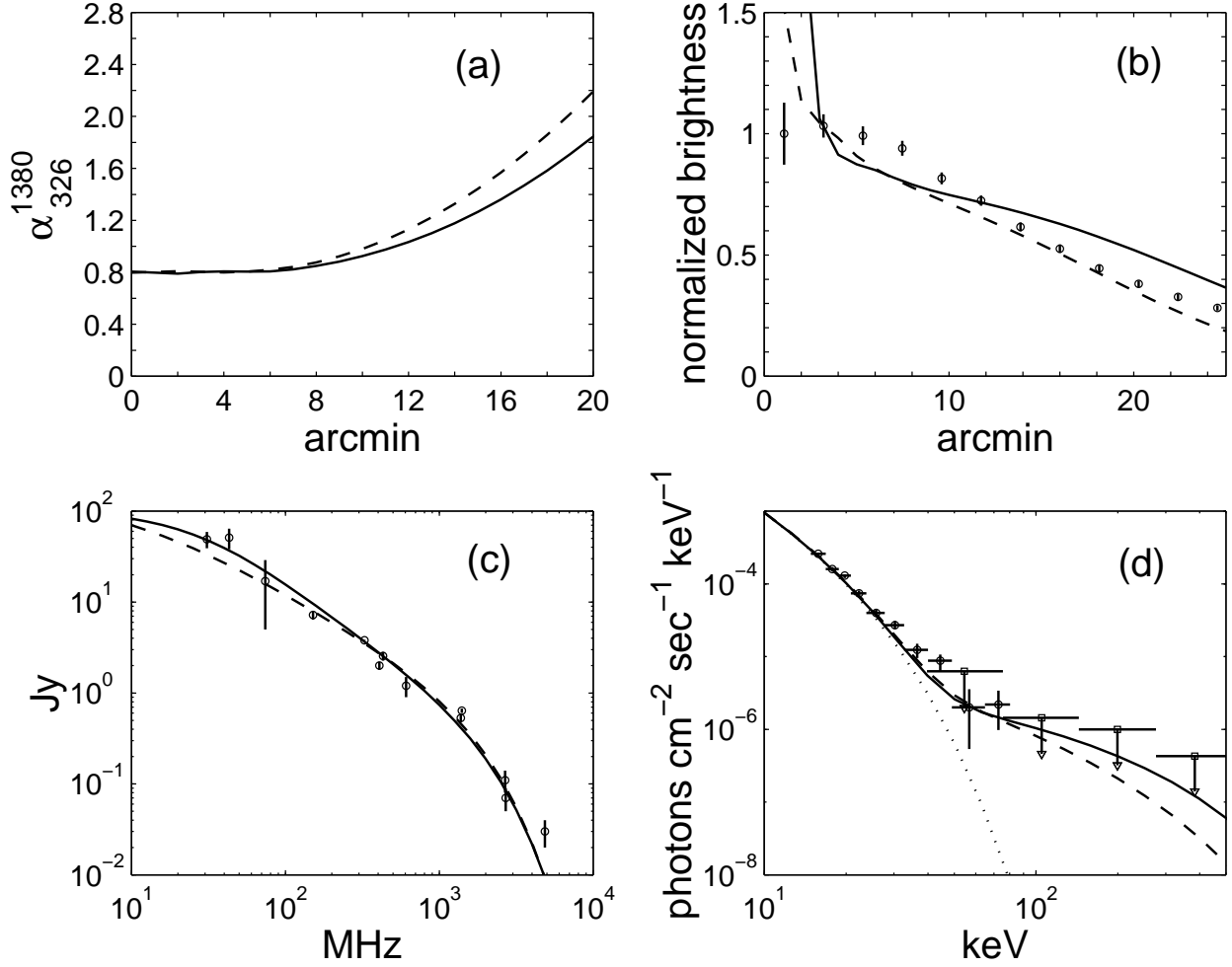


Fig. 6.— Time-dependent models with the power-law index  $s = 3.3$ , models B1 (*dashed curve*) and B2 (*solid curve*). (a) Spectral-index distributions. (b) Brightness distributions. (c) Integrated radio spectra. (d) HXR spectra.

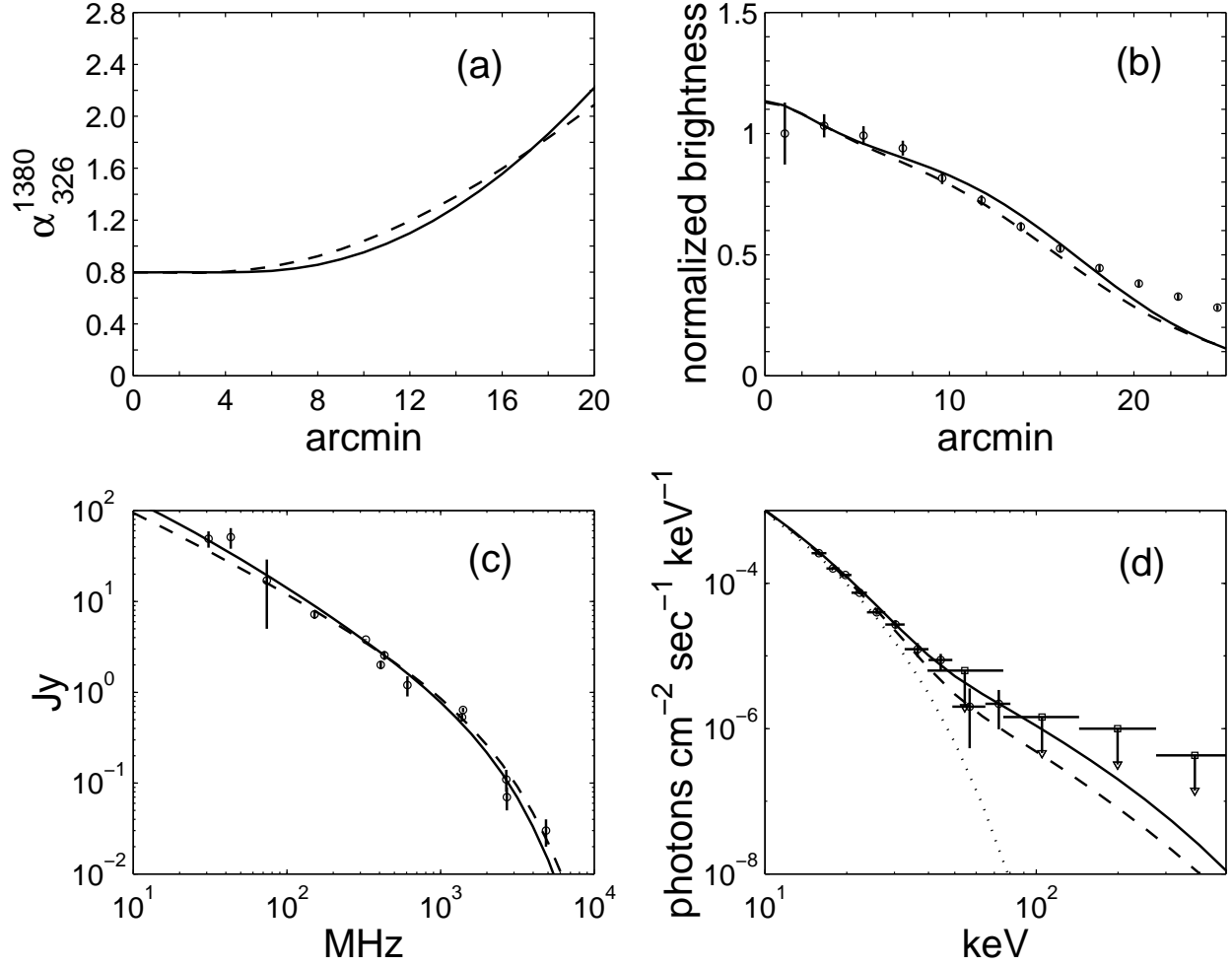


Fig. 7.— Time-dependent models with the power-law index  $s = 4.0$ , models B3 (*dashed curve*) and B4 (*solid curve*). (a) Spectral-index distributions. (b) Brightness distributions. (c) Integrated radio spectra. (d) HXR spectra.

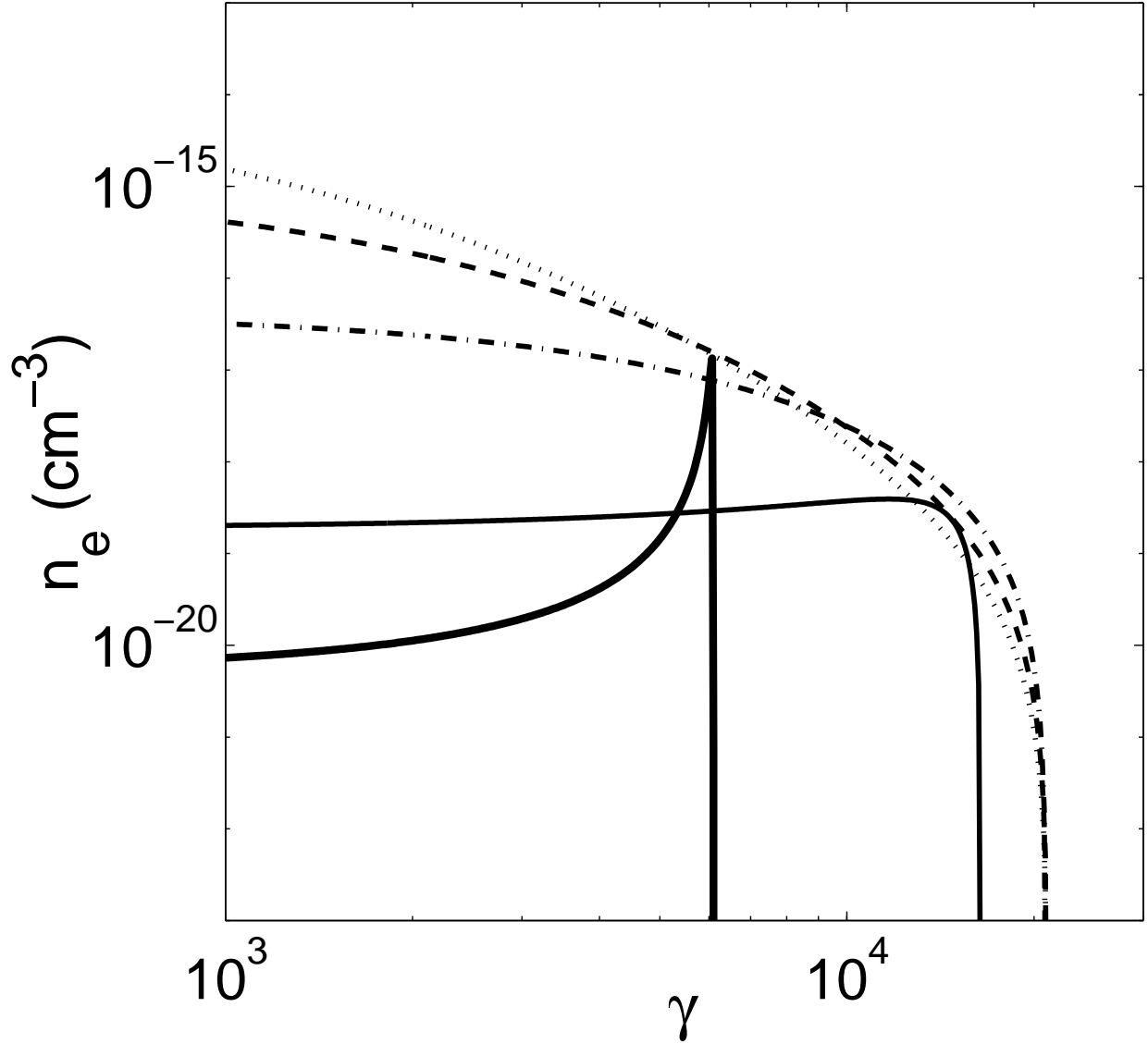


Fig. 8.— Electron spectra at different radii. The parameters are from model A6. The spectra at  $r = 0$  (*thick solid curve*),  $10'$  (*solid curve*),  $30'$  (*dash-dotted curve*),  $50'$  (*dashed curve*), and  $70'$  (*dotted curve*) are shown.

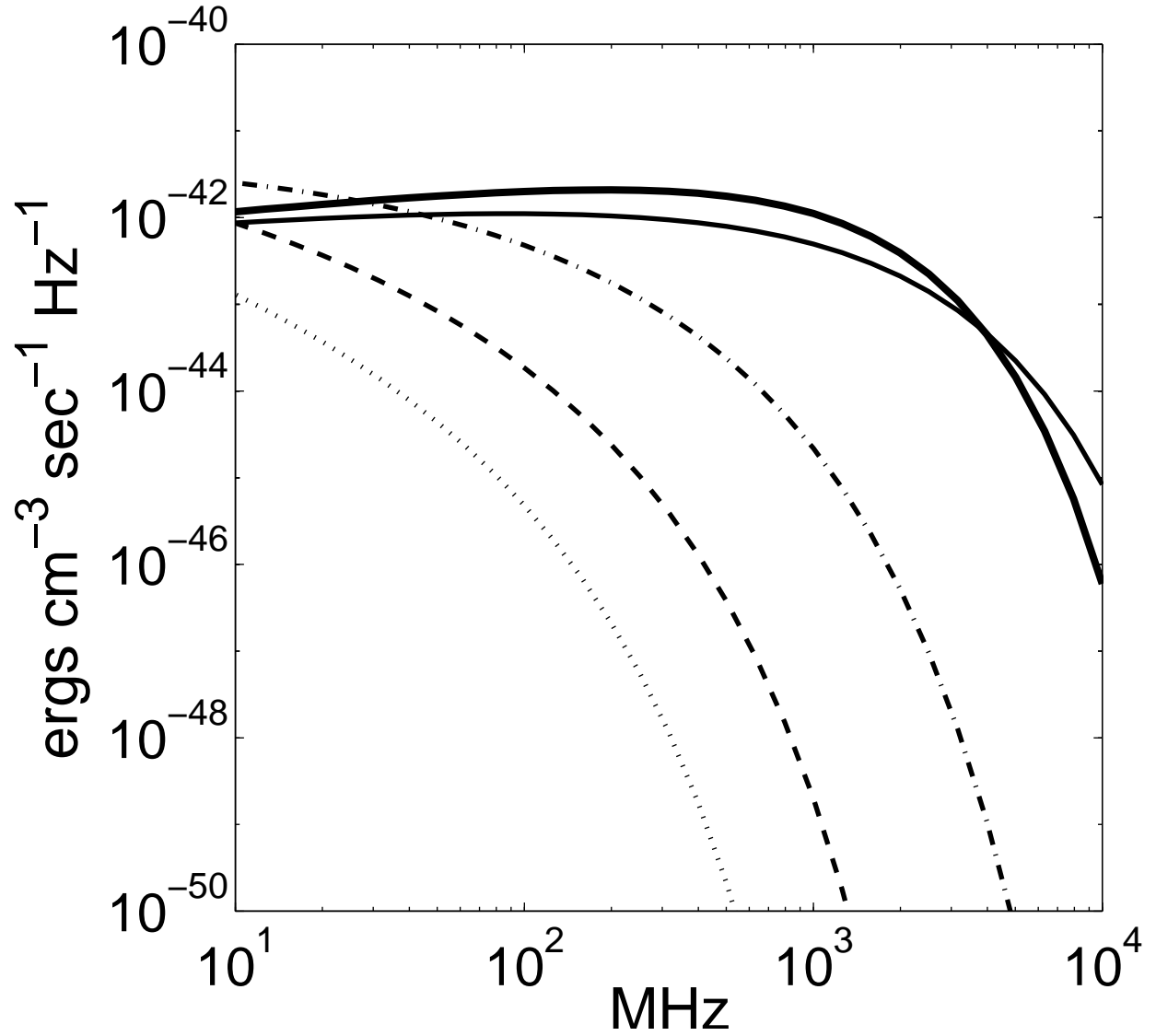


Fig. 9.— Radio emissivity at different radii. The parameters are from model A6. The emissivity at  $r = 0$  (*thick solid curve*),  $10'$  (*solid curve*),  $30'$  (*dash-dotted curve*),  $50'$  (*dashed curve*), and  $70'$  (*dotted curve*) are shown.

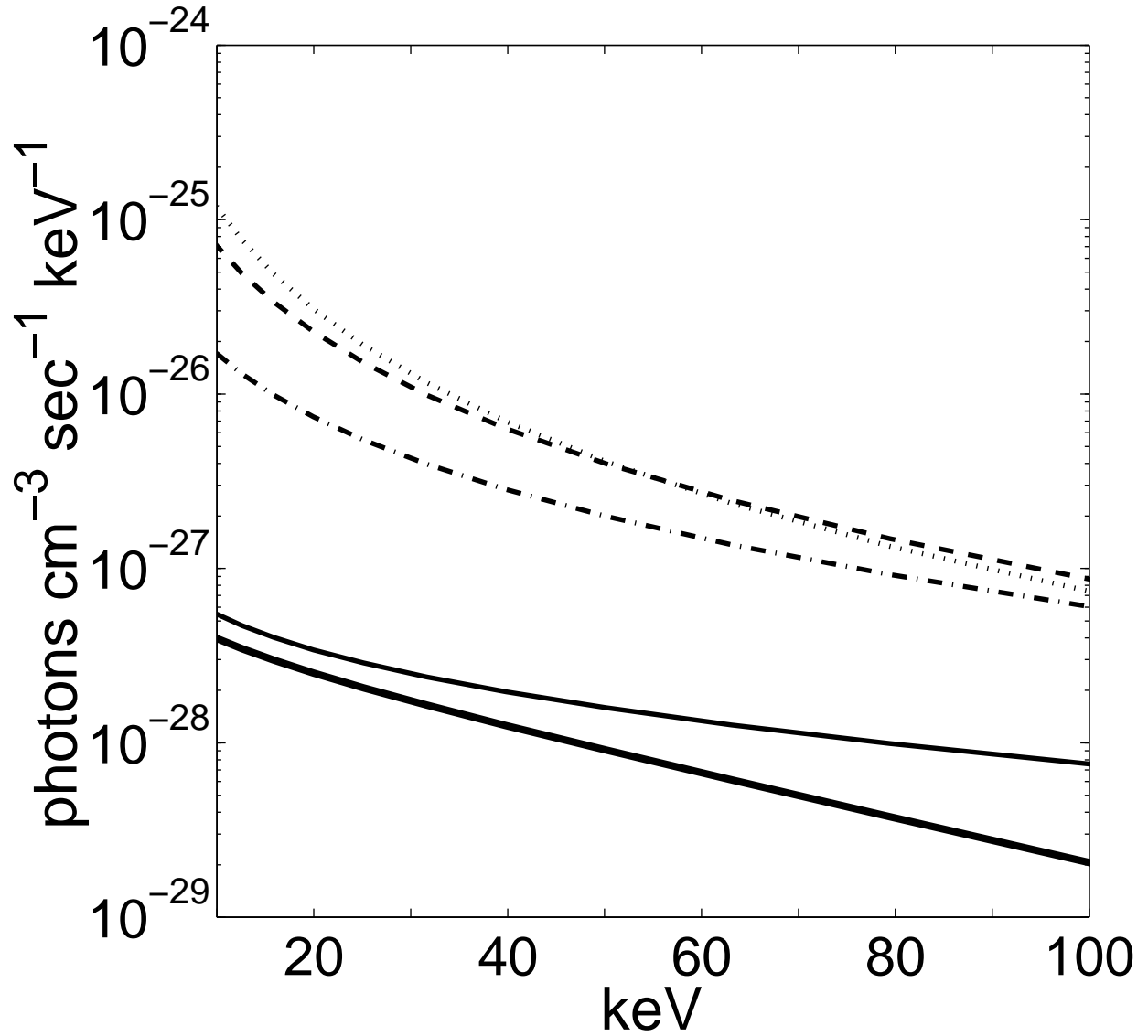


Fig. 10.— HXR excess emissivity at different radii. The parameters are from model A6. The emissivity at  $r = 0$  (*thick solid curve*),  $10'$  (*solid curve*),  $30'$  (*dash-dotted curve*),  $50'$  (*dashed curve*), and  $70'$  (*dotted curve*) are shown.